Technical Notes

TECHNICAL NOTES are short manuscripts describing new developments or important results of a preliminary nature. These Notes cannot exceed 6 manuscript pages and 3 figures; a page of text may be substituted for a figure and vice versa. After informal review by the editors, they may be published within a few months of the date of receipt. Style requirements are the same as for regular contributions (see inside back cover).

Unsteady Transonic Computations on Porous Aerofoils

C. P. Chen*
National Tsing Hua University, Taiwan, Republic of China
and
M. J. Sheu†
Optimal, Computer Aided Engineering, Inc., Michigan 48050

Introduction

THE inconvenience of supercritical aerofoils is the narrowness of the optimum Mach number and incidence range. When the region of the aerofoil surface where the shock waves occur is perforated, the pressure jump intensity across the shock wave on aerofoil can be reduced by using a secondary flow through the porous surface. Numerical algorithms to compute the unsteady form of full potential equation are still in a developmental stage, and the progress in the area has recently been made by several researchers.[1-5]

The governing equation, which describes the transonic flow around the aerofoil, is the unsteady full potential equation. A fully conservative formulation is applied on a moving body-fitted coordinate system. A numerical procedure is based on the local time field integral equation and the wake model, which was developed by Chen and Sheu[6] to solve the subcritical unsteady aerofoil problems.

In the present approach, a calculation procedure combining the internal integral equation method[7] and the finite-difference technique is adopted to compute full potential solution with large embedded supersonic regions and strong shocks. The integral equation method is integrated via Green's theorem to show that the velocity at any point in the field space can be expressed as the effects of distributions of source and vorticity on the mean camberline of aerofoil.

The grid on aerofoil surface is used to satisfy the boundary condition of zero normal flow across the aerofoil contour. The field grid need only be in a region where the strong shock wave occurs and the nonlinear compressibility effects cannot be neglected. The determination of the grid on the aerofoil surface and the field grid depends on the accuracy of the requirement; i.e., the choice of the number of elements on the field space and on the aerofoil contour is flexible.

The use of the internal singularity method needs fewer unknowns as compared to the surface singularity method.[7] The use of the present internal singularity distributions does not need to satisfy the requirement of the gap, which is placed between the leading edge and the element closest to the leading edge along the mean camberline. It takes much computer running time to decide the size of gap.[8]

A field source distribution, which is a function of the velocities and their derivatives, is used to represent the compressibility effects. The velocity derivatives on the transformed plane are calculated using finite-difference formulas enabling the introduction of artificial viscosity and upwind difference for the computation of supercritical flows. However, the derivatives on the physical plane are obtained by using the Jacobian of the transformation.

At each iterative procedure, the field source distribution is computed and results in additional induced velocities that disturb the tangency boundary condition on the aerofoil surface. The internal singularity distribution is determined at each iteration so that the tangency boundary condition can be satisfied. The nonlinear problem reduces to a Poisson equation at every iteration. The field source term is augmented by an artificial viscosity[9] term in the supersonic region to replace compression shock by a continuous narrow region of large velocity gradients.

The experimental data and the numerical solutions are not available for the porous aerofoils in unsteady transonic flows. Therefore, the results of the porous aerofoil are compared to those of solid aerofoil to show the effect of the porosity on the pressure distribution. The numerical solutions of solid aerofoil are presented at the reduced frequency of 0.162 so that a comparison of the present solution can be made with experimental data.[10] The application of NACA 0012 aerofoil is used to calculate the unsteady pressure distribution, lift, and pitching moment in pitching oscillation.

Mathematical Analysis

The governing equation in the coordinate system (x,y,t) is transformed to a local coordinate system (ξ,η,τ) in which the moving body-conforming mesh is generated. The O-type grid generation is used to provide smoothly body fitted. The details of the numerical procedure for solid aerofoil can be found in Refs. 6, 7, and 8.

The normal velocity on the porous aerofoil surface is determined from the Darcy's law, which states that the normal velocity (V_n) on the porous surface is proportional to the pressure gradient (ΔP) between its two sides, i.e.,

$$V_n = b\Delta P \tag{1}$$

and

$$b = \frac{\hat{b}}{\rho_\infty V_\infty} \tag{2}$$

where porosity fraction $\hat{b}$ is a function of the hole size.

The pressure gradient can be determined by the unsteady energy equation, and if the pressure inside the porous surface is not equal to the freestream pressure, i.e., $P_i \neq P_\infty$, Eq. (1) becomes

$$V_n = \frac{\hat{b}V_\infty(M_\infty^2)^{1/(\gamma-1)}}{\gamma}[(a_i^2)^{\gamma/(\gamma-1)} - (a_0^2)^{\gamma/(\gamma-1)}] \tag{3}$$

where a_i and a_0 are the local speeds of sound at the adjacent points internal and external to the aerofoil surface respec-

Received July 10, 1989; revision received Nov. 27, 1989.

*Postgraduate Student, Department of Power Mechanical Engineering.

†Research Engineer. Member AIAA.

tively. V_∞ and M_∞ are the freestream velocity and Mach number. The γ is the ratio of specific heats ($=1.4$). The overall air mass flow rate (Q) over the entire porous surface must be zero, i.e.,

$$Q = \int_s \rho V_n \, ds \tag{4}$$

The tangential velocity inside the porous aerofoil surface can be obtained by solving Eqs. (3) and (4),

$$(a_i^2)^{(\gamma+1)/(\gamma-1)} = \left[\int_s \hat{b}(a_0^2)^{(\gamma+1)/(\gamma-1)} \, ds\right] \Big/ \left[\int_s \hat{b} \, ds\right] \tag{5}$$

The boundary condition to be satisfied on the porous aerofoil surface is

$$(V_\infty + U)\eta' + V = V_n \tag{6}$$

where U and V are the velocity components in the ξ- and η-axes on the aerofoil surface. The η' is the slope of the aerofoil surface at time $\tau_k \cdot V_\infty$ is the freestream velocity. The porosity distribution function is given by

$$\hat{b} = \hat{b} \max\left[\sin \frac{\xi - \xi_1}{\xi_2 - \xi_1} \pi\right] \tag{7}$$

where the region of porous surface starts from 0.2 to 0.9 chord length.

If the pressure inside the porous surface is equal to the freestream pressure, i.e., $P_i = P_\infty$, Eq. (1) becomes

$$V_n = \frac{\hat{b} V_\infty}{\gamma}[a_\infty^2 - (M_\infty^2)^{1/(\gamma-1)}(a_0^2)^{\gamma/(\gamma-1)}] \tag{8}$$

where a_∞ is freestream speed of sound. The iterative procedure to solve the flowfield of porous aerofoil is

1) For the calculation of porous aerofoil, the initial input sets up the unsteady solutions of solid aerofoil about the mean position then performs the unsteady porous aerofoil. The value of $\hat{b}$ is determined from Eq. (7).

2) If $P_i = P_\infty$, then a_i can be obtained by Eq. (5) and a_0 can be given by the conservation of energy.

3) The solutions of step 2 are substituted into Eq. (3) to determine the value of V_n if $P_i \neq P_\infty$. However, if $P_i = P_\infty$, the value of V_n is given by solving Eq. (8).

4) The new boundary condition is given by the contributions of the freestream velocity (V_∞), the strengths of field source (σ_f), the strengths of the vortices in the wake (γ_ω), and the value of V_n, which is obtained from step 3. The determination of these singularities can be found in the calculation of solid aerofoil.

5) Repeat steps 2 to 4 until the convergence of boundary condition [i.e., Eq. (6)] is obtained within the error of tolerance 1×10^{-3}.

Results and Discussions

The results of NACA 0012 aerofoil in pitching motion are presented to show the effect of the porosity on the unsteady pressure distribution, lift, and pitching moment. The condition for the oscillation is given as $M_\infty = 0.755$, $\alpha_m = 0.02$ deg, $\alpha_0 = 2.59$ deg, $\omega = 0.162$, and the angle of oscillation is defined as $\alpha = \alpha_m + \alpha_0 \sin(\omega t)$ so that the numerical solution can be compared with those of experimental data obtained from AGARD R-702.[10] All the cases are calculated by using the CDC 840 computer system with the O-type mesh of 50×12. The calculation takes approximately 55–60 min computer CPU running time.

Figures 1–4 show the unsteady results on NACA 0012 at reduced frequency $\nu = 0.162$ (where $\nu = \omega c / V_\infty$). Figure 1 shows unsteady pressures on the surface of the pitching aerofoil. Figure 2 shows the unsteady variation in lift coefficient; the results in pitching moment coefficient (about a quarter chord) are shown in Fig. 3. In all of these results, the agreement between numerical solution and experimental data is excellent. The pressure jump across the shock wave can be reduced by using the porous aerofoil. The pressure distribution on the aerofoil surface at $x/c \leq 0.6$ for the case of $P_i \neq P_\infty$ is greater than that for the case of $P_i = P_\infty$. However, aft of the region at $x/c \geq 0.6$, the pressure distribution on the surface for the case of $P_i = P_\infty$ is greater than that for the case of $P_i \neq P_\infty$. The lift coefficient for the porous aerofoil is a little shift when comparison is made with that of the solid aerofoil. The pitching moment coefficient for the porous aerofoil is different from that of the solid aerofoil. Figure 4 shows the location of shock wave which is a function of angle of incidence.

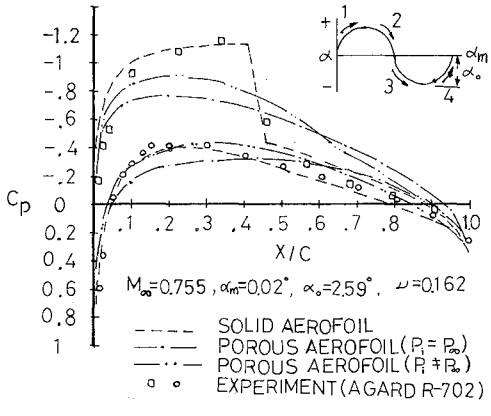

Fig. 1 Comparison of pressures, $\alpha(t) = -2$ deg during upswing.

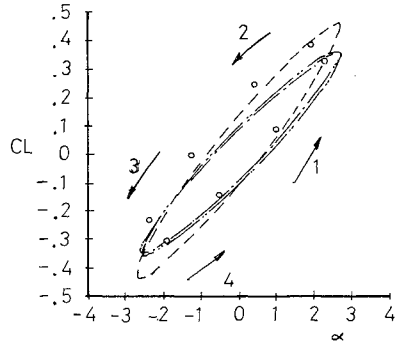

Fig. 2 Comparison of lift coefficient.

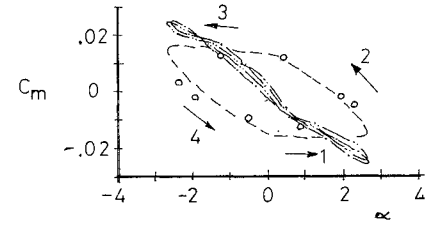

Fig. 3 Comparison of pitching moment coefficient.

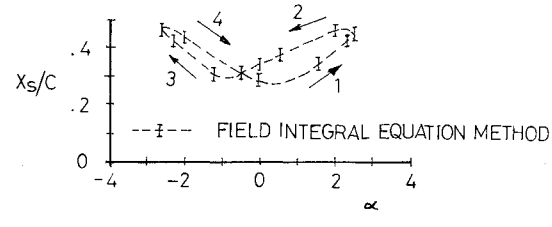

Fig. 4 Unsteady shock locations.

Conclusions

This Note presents a numerical scheme based on an integral approach, which is extended and modified to present sub-critical integral equation method and the wake model to transonic oscillatory solid and porous aerofoils in pitching motion. This method is able to capture reasonably sharp shocks spread over the aerofoil surface, whose strengths and locations agree well with the experimental data. The present approach shows that the use of a compressible linear operator with the addition of artificial viscosity to the governing equation is sufficient to produce convergence for the cases arising in inviscid isentropic flows with shocks.

References

[1]Steger, J., and Caradonna, F., "A Conservative Implicit Finite Difference Algorithm for the Unsteady Transonic Full Potential Equation," AIAA Paper 80-1368, July 1980.

[2]Malone, J. B., and Sankar, N. L., "Numerical Simulation of Two-Dimensional Unsteady Transonic Flows Using the Full Potential Equation," AIAA Paper 83-0233, 1983.

[3]Shankar, V., Ide, H., Gorski, J., and Osher, S., "A Fast Time Accurate, Unsteady Full Potential Scheme," *AIAA Journal*, Vol. 25, No. 2, Feb. 1987, pp. 230–238.

[4]Hounjet, M. L., "Calculation of Unsteady Transonic Flows with Shocks by Field Panel Methods," *AIAA Journal*, Vol. 20, No. 6, June 1982, pp. 857–859.

[5]Hounjet, M. H. L., "A Field Panel/Finite Difference Method for Potential Unsteady Transonic Flow," *AIAA Journal*, Vol. 23, No. 4, April 1985, pp. 537–545.

[6]Chen, D. R., and Sheu, M. J., "Numerical Solutions for Oscillatory Aerofoil at High Reduced Frequency," *Computer Methods in Applied Mechanics and Engineering*, Vol. 74, No. 1, Sept. 1989, pp. 55–68.

[7]Chen, D. R., and Sheu, M. J., "Comparison of Numerical Solutions of Lower and Higher Order Integral Equation Methods for Two-Dimensional Aerofoils," AIAA Paper 86-2591, Sept. 1986.

[8]Chen, D. R., and Sheu, M. J., "An Investigation of Internal Singularity Methods for Multi-Element Airfoils," *Journal of Aircraft*, Vol. 26, No. 2, Feb. 1989, pp. 189–192.

[9]Jameson, A., "Iterative Solutions of Transonic Flows Over Airfoils and Wings, Including Flows at Mach 1," *Communications on Pure and Applied Mathematics*, Vol. 27, 1974, pp. 283–309.

[10]"Compendium of Unsteady Aerodynamic Measurements," AGARD R-702, Aug. 1982.

Nonlinear Static and Dynamic Analysis Method of Cable Structures

Jin Mitsugi* and Tetsuo Yasaka†
Nippon Telegraph and Telephone Corporation
Radio Communication System Laboratories,
Yokosuka, Japan

Introduction

CABLES are very promising structural elements for space applications since they can be packaged easily in a small volume and function as truss members when in a stretched state.[1] However, an exact analysis of cable structures is difficult because of cable slackening and large deformations. This is particularly true when the cables form a network. Usually cables are modeled as pin-supported rods, and a linear, finite element analysis is employed.[2] If all the cables are in tension and the number of cables is greater than or equal to the degrees of freedom of the structure, a linear, finite element analysis gives a good approximation. However, if any cables are slack and/or the structure is a tension stabilized structure, an iterative technique has to be employed in a linear analysis. Herbert and Bachtell[3] reported a nonlinear analysis method that includes second-order strains and the effect of tension stabilization, but higher-order strains and the effect of cable slackening were neglected.

In this Note, a nonlinear cable structure analysis method is derived based on Hamilton's principle and a general purpose cable structure analysis code (CASA) is developed. Higher-order strains are included in the method by taking positions, not displacements, as variables, and cable slackenings are given by a nonlinear, axial stiffness of cable. Nonlinear static and linear dynamic analyses of structures composed of cables and/or trusses can be treated by the present method.

Theory

Assume that the number of elements (cables or trusses) in the structure is C and the number of nodes is n. The strain energy in the structure is expressed by the summation of the strain energy in each element

$$P=\sum_{i=1}^{c}\frac{1}{2}\left(\frac{|\bar{X}_{i1}-\bar{X}_{i2}|-1_{0i}}{1_{0i}}\right)^2(EA)_i 1_{0i} \tag{1}$$

where 1_{0i} denotes the initial length (length in nonstressed state) of ith element and $(EA)_i$ denotes the axial stiffness (product of Young's modulus and cross-sectional area) of ith element. $\bar{X}_{i1}$ and $\bar{X}_{i2}$ denote the position vectors of two terminal nodes of ith element. The axial stiffness $(EA)_i$ of a cable element is set to zero when the strain is negative. The strain energy variation corresponding to the node position variations is given as

$$\delta P=\sum_{i=1}^{c}\frac{(EA)_i(|\bar{X}_{i1}-\bar{X}_{i2}|-1_{0i})}{1_{0i}|\bar{X}_{i1}-\bar{X}_{i2}|}(\bar{X}_{i1}-\bar{X}_{i2})\cdot(\delta\bar{X}_{i1}-\delta\bar{X}_{i2}) \tag{2}$$

An external force of magnitude f_j is imposed on the jth node from a fixed node, whose position vector is $\bar{X}_{fj}$. The virtual work is given as

$$\delta W=\sum_{j=1}^{n}f_j\frac{(\bar{X}_{fj}-\bar{X}_j)}{|\bar{X}_{fj}-\bar{X}_j|}\delta\bar{X}_j \tag{3}$$

Combining the variation of potential energy and the virtual work, according to the principle of stationary value of the total potential energy, yields

$$\bar{F}_1\cdot\delta\bar{X}_1+\bar{F}_2\cdot\delta\bar{X}_2+\ldots\bar{F}_n\cdot\delta\bar{X}_n=0 \tag{4}$$

where $\bar{F}_i$ is a nonlinear function of vectors $\bar{X}_i$. When the number of fixed nodes is n_f, the nonlinear equations that describe the static equilibrium state are given as follows:

$$\begin{cases}\bar{F}_1(\bar{X}_1,\bar{X}_2,\ldots\bar{X}_m)=0\\ \vdots\\ \bar{F}_m(\bar{X}_1,\bar{X}_2,\ldots\bar{X}_m)=0\end{cases} \tag{5}$$

where $m=n-n_f$. Solving Eq. (5) using the Newton-Raphson method yields the static equilibrium state of the structure. The

Received Sept. 11, 1989; revision received Dec. 11, 1989; accepted for publication Dec 13, 1989.

*Research Engineer, Communication Satellite Technology Laboratory.

†Executive Research Engineer, Communication Satellite Technology Laboratory. Member AIAA.